Proceedings of the 11th Brazilian Congress of Thermal Sciences and Engineering -- ENCIT 2006
Braz. Soc. of Mechanical Sciences and Engineering -- ABCM, Curitiba, Brazil,- Dec. 5-8, 2006

Paper CIT06-0313

PHYSICAL ASPECTS OF THE FLOW OVER SHALLOW CAVITIES: A NUMERICAL INVESTIGATION

P.S.B. Zdanski
Department of Mechanical Engineering
State University of Santa Catarina
89223-000 – Joinville – SC - Brazil
zdanski@joinville.udesc.br

M.A. Ortega
Department of Aeronautical Engineering
Technological Institute of Aeronautics
12228-900 – São José dos Campos – SP - Brazil
ortega@ita.br

N.G.C.R Fico Júnior
Department of Aeronautical Engineering
Technological Institute of Aeronautics
12228-900 – São José dos Campos – SP – Brazil
nide@ita.br

Abstract. *The flow over shallow cavities is numerically investigated. The analysis is performed for both, laminar and turbulent regimes. Some interesting features, previously detected, are discussed on the physical basis. The results obtained demonstrate that the vorticity shed at the upstream corner and the stagnation region formed at the downstream vertical wall dictate the physical scenario in terms of flow topology inside the cavity for both turbulent and laminar regime. The heat transfer budget for the turbulent cavity revealed an interesting feature of the convection fluxes inside the cavity, e.g., a symmetric behaviour. The mathematical model corresponds to the incompressible, Reynolds-averaged, Navier-Stokes equations plus a two-equation k-e turbulence model. Two numerical schemes are adopted in the analysis. The SIMPLER method, based in finite volume formulation, is used in the laminar study. Otherwise, for turbulent analysis, a finite difference scheme that has recently been developed by the present authors was applied.*

Keywords*. Shallow cavities, incompressible flows; numerical methods*

1. Introduction

The flow over cavities is of great practical interest, being extensively studied with the aim of analyze solar energy collectors, combustion chambers and environmental problems. Previous work, by the present authors, revealed some interesting aspects about this kind of flow, i.e., the opposite behavior on the displacement of the vortices inside the cavity for laminar and turbulent regimes (Zdanski et al., 2003), and the role played by the turbulent diffusion upon heat transfer rate at the cavity floor (Zdanski et al., 2005). These features were not fully explored on its physical aspects. Thus, the main goal here is to discuss these issues in more detail.

The flow inside cavities is characterized by the appearance of large re-circulation regions. The literature data available is mainly devoted to the analysis of deep cavities and there is little information about cavities of large aspect ratios, or shallow cavities. Sinha et al. (1982) have reported experimental results for deep cavities as well as for shallow ones. This particular work reveals some important aspects about flow topology inside shallow cavities, but only for the laminar case. Frigo et al. (2004) presents numerical results for transient flow in free cavities with aspect ratios 1 and 2. This work emphasizes the analysis of time evolution of streamlines and velocity profiles inside the cavity. For a more complete review about this topic the reader may access the works of Zdanski et al. (2003, 2005).

The numerical analysis was performed with two distinct schemes, i.e., the SIMPLER algorithm (Patankar, 1980) and the one developed by the present authors (Zdanski et al., 2004). The SIMPLER method is completely standardized in the literature and the other scheme adopts central difference formulas to discretize both convective and diffusive terms in a collocated mesh. To control odd-even decoupling problem, artificial viscosity terms are added externally. The laminar flow simulations were obtained through the SIMPLER algorithm while all turbulent cases were simulated with our "in-house" code. Although not shown here some laminar cases were re-calculated with the new method and the results were very similar to the ones obtained by the classical Patankar's algorithm. That is, all major flow characteristics were recovered, thus, ruling out the possibility that the numerical scheme is a determinant factor on the flow aspects discussed hereafter. Further, a careful mesh refinement study was performed yielding grid-independent results. The results obtained demonstrate that vorticity shed at the cavity corner has the major influence upon the

bubbles position inside the cavity. Another result, related to heat transfer budget, indicates a symmetric behavior on the convection fluxes inside the cavity.

An important point that should be clear is that ours is essentially an engineering approach. Therefore, the interest lies on the steady mean flow. We are aware that the dynamics inside the cavity is extremely complicated, and that the instantaneous flow plays a very important role. But, the emphasis of this paper is on the engineering aspect of the problem.

2. Theoretical formulation

2.1. Governig equations

The flow is modeled by the two-dimensional, Cartesian, incompressible, Reynolds-averaged, continuity, Navier-Stokes, and energy equations. In the Einstein notation the equations can be written as

$$\frac{\partial U_j}{\partial x_j} = 0 \,, \tag{1}$$

$$\frac{\partial(\rho U_i)}{\partial t} + \frac{\partial(\rho U_j U_i)}{\partial x_j} = -\frac{\partial p}{\partial x_i} + \frac{\partial}{\partial x_j}\left(2\mu S_{ij} - \rho\overline{u_i' u_j'}\right), \tag{2}$$

$$\frac{\partial(\rho c_p T)}{\partial t} + \frac{\partial(\rho c_p U_i)}{\partial x_i} = \frac{\partial}{\partial x_i}\left(\kappa\frac{\partial T}{\partial x_i} - \rho c_p \overline{u_i' T'}\right), \tag{3}$$

where the mean strain rate is given by

$$S_{ij} = \frac{1}{2}\left(\frac{\partial u_i}{\partial x_j} + \frac{\partial u_j}{\partial x_i}\right). \tag{4}$$

For modeling the turbulent flow, we have adopted the Boussinesq approximation, where the turbulent fluctuations are correlated to mean flow properties as

$$-\rho\overline{u_i' u_j'} = \mu_T\left(\frac{\partial U_i}{\partial x_j} + \frac{\partial U_j}{\partial x_i}\right) - \frac{2}{3}\delta_{ij}\rho k \,, \tag{5}$$

$$-\rho c_p \overline{u_i' T'} = \kappa_T \frac{\partial T}{\partial x_i} \,, \tag{6}$$

being μ_T and κ_T the turbulent eddy viscosity and turbulent thermal conductivity, respectively. For computation of turbulent viscosity it was adopted the standard κ-ε turbulence model (Launder and Spalding, 1974). For determination of the turbulent thermal conductivity we have adopted the definition of constant Prandtl turbulent number, i.e., $P_{rT} = 0.9$.

2.2. Numerical method

The numerical scheme adopted for the laminar analysis was the SIMPLER algorithm (Patankar, 1980). Otherwise, for the turbulent studies, the method developed by the present authors (Zdanski et al., 2004) is employed. The SIMPLER scheme is completely standardized in literature, while the other scheme is a recent proposal. The novel method discretizes the equations in a collocated mesh with central difference formulas. Artificial smoothing terms are added to control the odd-even decoupling and non-linear instabilities. The equations, written in conservation law form, are solved implicitly. A Poisson equation for pressure is solved to assure free divergence for velocity field. Distinctly of traditional pressure-correction methods, the convergence of the present scheme is assured without resorting to any kind of relaxation parameters. For more details about the scheme the reader is addressed to reference Zdanski et al. (2004).

3. Results and discussions

3.1 Problem statement and boundary conditions

The shallow cavity with the main dimensions is depicted at fig. (1). Boundary conditions were enforced as follows: at the inlet plane distributions of velocity, temperature, turbulent kinetic energy and turbulent dissipation rate are specified. The parabolic condition was enforced for all variables at the exit section. At the upper boundary coupling with the free stream flow is used. At solid walls the condition of zero velocity was enforced and the shear stress and heat flux are obtained from the law of the wall (Mansour et al., 1983) together with the standard κ-ε model (Launder and Spalding, 1974). The values of pressure and turbulent kinetic energy at the wall are obtained by a zero-order extrapolation from the values at the first cell.

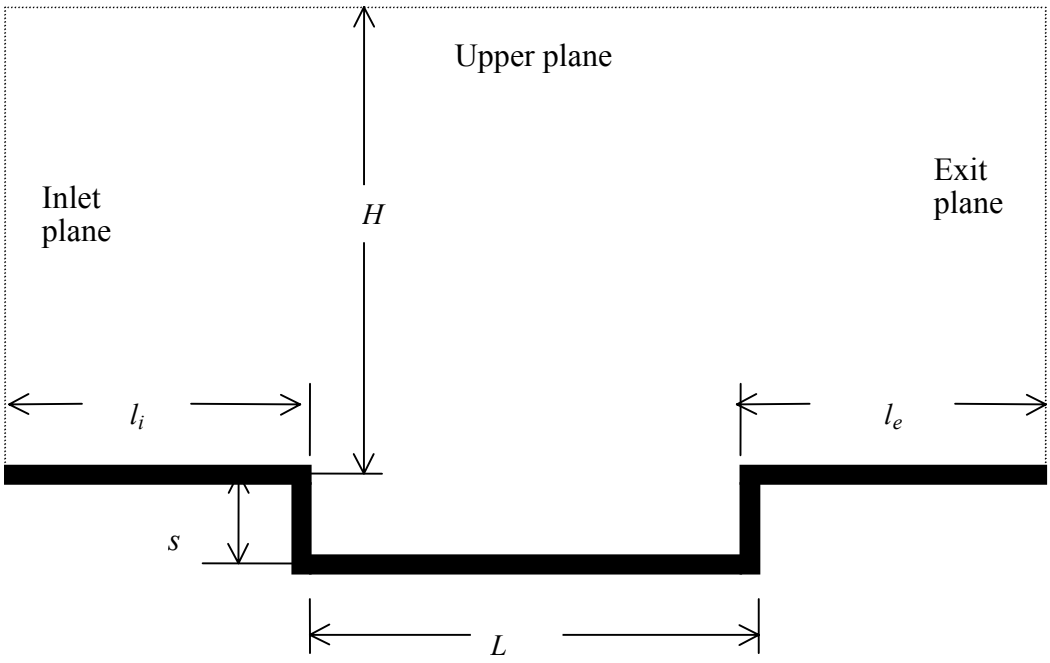

Figure 1. Shallow cavity with the main dimensions.

The codes used in the present analysis were extensively tested in previous works (Zdanski et al., 2003, 2004, 2005). Comparisons with experimental and theoretical literature data have ever been satisfactory. These facts corroborate for the credibility of the results presented herein. A typical computational mesh used in the cavity analysis presents points clustering close to solid walls and to the horizontal plane connecting the two corners. The first grid point is set at $y^+ \approx 30$ (for turbulent flow), and the maximum stretching factor for the mesh was 9%.

3.2 Displacement of the vortices inside the cavity

It was discovered in the authors' previous work (Zdanski et al., 2003) that the Reynolds number affects the bubbles position inside the cavity for the laminar and turbulent regime. In the laminar case, for lower velocities, we have the flow reattached at the cavity floor, and the two bubbles encapsulate for higher velocities (Zdanski et al., 2003). This is so because increasing Reynolds number causes the greater bubble displaces in the downstream direction (Zdanski et al., 2003). Otherwise, for the turbulent regime, the opposite occurs, i.e., the bubbles are encapsulated for lower velocities and the flow reattaches at the cavity floor with higher velocities (Zdanski et al., 2003, 2005). Furthermore, for the turbulent flow the bubble center does not change the position with increasing Reynolds number (Zdanski et al., 2005). What is the reason for this fact? This paper aims at understanding better this physical scenario.

The aspect ratios considered for the present analysis were equals to 8 for the turbulent case and 12 for the laminar flow. These values were chosen to ensure the formation of two vortexes inside the cavity. The variation of the Reynolds number, based upon the cavity depth Re_s, was a consequence of the variation of the entrance velocity. For the turbulent case, values of U_{in} equal to 5m/s, 8m/s, and 12m/s, corresponding to Re_s equal to 13285, 21255, and 31880, are simulated. For the laminar regime we have adopted U_{in} equal to 0.4 m/s, 0.8m/s, 1.2m/s, and 1.8m/s corresponding to Re_s=147, 294, 442 and 662, respectively.

In Table (1), it is represented the vorticity (evaluated as U_{in}/δ) for the velocities tested. This quantity was calculated at the cavity upstream corner, where the boundary layer separates. The first conclusion, 'the obvious one' was that for higher velocities we have more vorticity being shed at the cavity corner. The most important conclusion can be drawn from figs. (2) and (3), where the pressure distribution along the cavity floor is represented. The values of pressure shown in these figures are dimensional, representing the differences between the pressure at a particular station along the cavity floor and the pressure at the inlet section. It can be realized that for the turbulent regime, increasing the Reynolds number will cause the pressure decreases at the greater bubble region ($x/s < 4.0$) and augments in the region near the downstream vertical face ($x/s > 4.0$). The physical scenario that explain this behavior is as follows: increasing Reynolds number will leads to higher vorticity (see Table (1)), thus lowering the pressure at the bubble center and, as a consequence, at the cavity floor ($x/s < 4.0$). Moreover, the pressure increase for $x/s > 4$ is linked to the flow stagnation that occurs at the downstream vertical face. Therefore, in the region $x/s > 4$, the higher vorticity effect is overwhelmed by the pressure rise due to flow stagnation. This pressure distribution can explain why, in the turbulent regime, the greater bubble does not change its position with increasing velocities. In effect, the net pressure force augments in downstream direction forcing the bubble against the upstream vertical cavity wall. Figure (3), representing the laminar case, show a rather distinct picture. Increasing the velocities (and consequently vorticity) will lead to a pressure decrease along the whole cavity floor. Therefore, the effect of vorticity is more important, overwhelming the pressure increasing caused by the stagnation region. Although the net pressure force increases, in the downstream direction, the gradient is much smaller than in turbulent case, permitting the greater bubble to move downstream (Zdanski et al., 2003). The major conclusion is the following: for the turbulent regime the vorticity being shed at the cavity corner is higher but their influence is restricted to the greatest bubble region ($x < 4$), and the pressure gradient does not permit the greater bubble to change the position with increasing Reynolds number. However, for the laminar case, the vorticity increasing, which causes a pressure decrease, is felt along the entire cavity floor. Thus, the pressure driven force is lower and the greater bubble moves downstream with increasing velocities.

Table (1) – Cavity corner vorticity as a function of Reynolds number, Re_s

Re_s	Vorticity (s^{-1})	Re_s	Vorticity (s^{-1})
147	45.13	13285	1178.50
294	93.35	21255	1867.92
442	144.10	31883	2700.00
662	229.12		

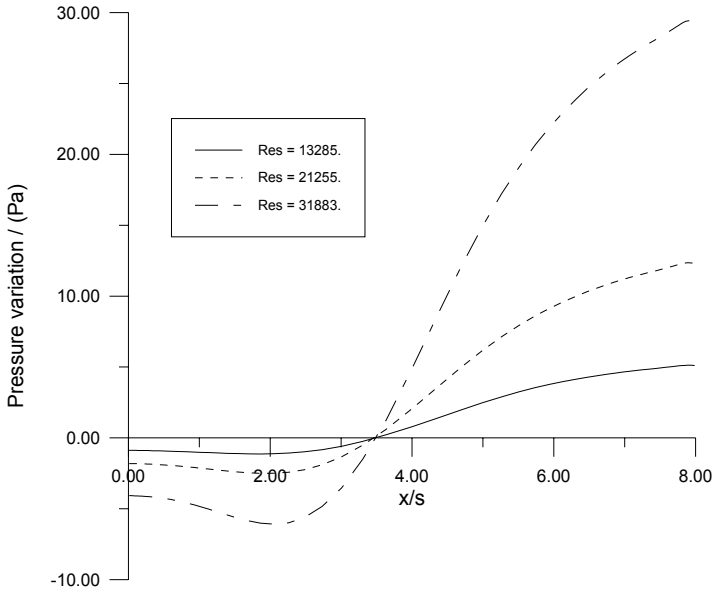

Figure 2. Pressure difference between the floor and the entrance section for cavity with (w/s) = 8

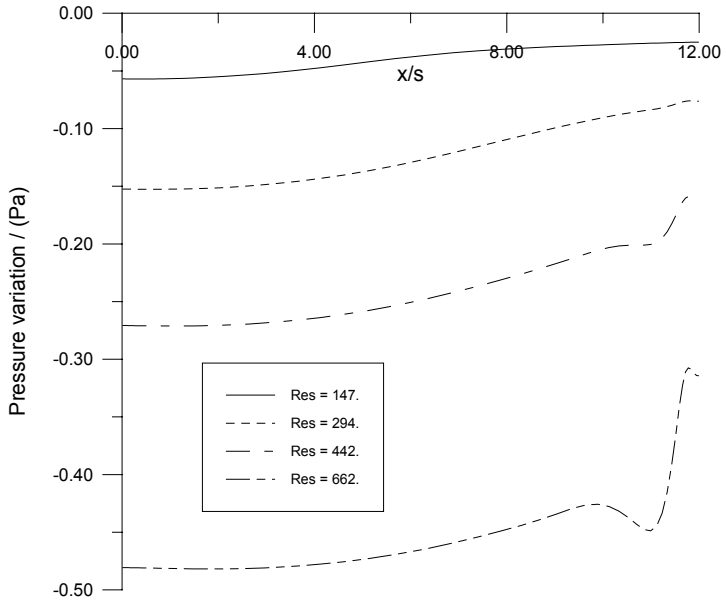

Figure 3. Pressure difference between the floor and the entrance section for cavity with (w/s) = 12

Aiming at better understanding the phenomenon the non-dimensional vorticity is plotted in figs. (4) and (5), i.e.,

$$Vorticity = \left(\frac{s}{U_{in}}\right)\left[\frac{\partial v}{\partial x} - \frac{\partial u}{\partial y}\right]. \tag{7}$$

The attention is focused at the cavity region. The fig. (4) presents results for a laminar simulation where Re_s = 442 whereas fig. (5) represents the turbulent picture for Re_s = 21,255. Clearly, we can realize that for turbulent flow the vorticity diffusion processes is more intense. Otherwise, if one analyzes the region near the cavity floor the immediate conclusion is the following: for turbulent flow we have the maximum positive vorticity near upstream step (x/s < 2) whereas for laminar flow this maximum vorticity region extends basically for the whole cavity floor. This observation is in agreement with the pressure distributions presented in figs. (2) and (3).

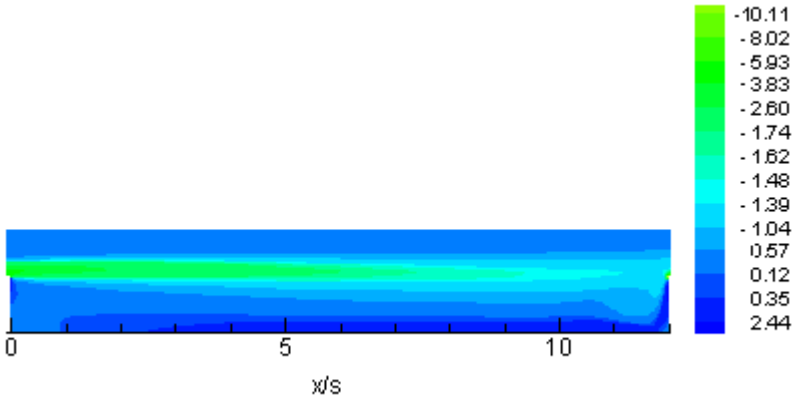

Figure 4. Vorticity distribution for laminar flow regime with (w/s) = 12.

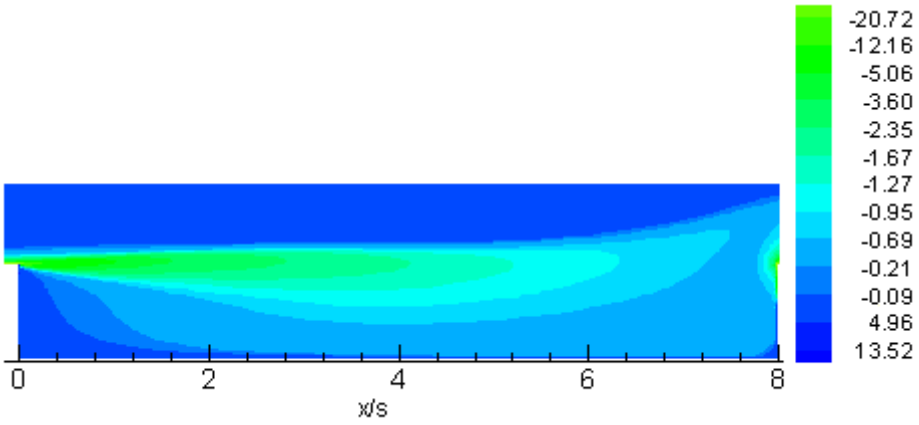

Figure 5. Vorticity distribution for turbulent flow regime with (w/s) = 8.

3.3 Heat transfer budget inside the cavity

It was demonstrated by the authors (Zdanski et al., 2005) that heat flux at the cavity floor is related to turbulent diffusion near cavity floor. Aiming a better understand of the phenomenon, we present the heat transfer budget inside the cavity. The convection and diffusion terms of the energy equation are evaluated at control volumes taken along the cavity length, as shown in fig. (6).

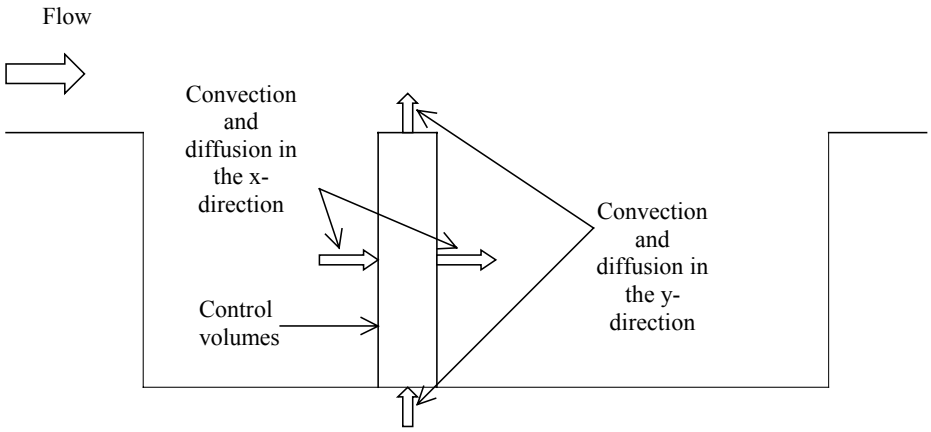

Figure 6. Control volume representation for heat transfer budget.

The integration of energy equation over the control surfaces leads to

$$\textit{Net x-convection} = \left[\left(\rho u c_p T\right)_{i+1/2} - \left(\rho u c_p T\right)_{i-1/2}\right]\Delta y\,,$$

$$\textit{Net y-convection} = \left[\left(\rho v c_p T\right)_{j+1/2} - \left(\rho v c_p T\right)_{j-1/2}\right]\Delta x\,,$$

$$\textit{Net x-diffusion} = \left[\left(\kappa_{eq}\frac{\partial T}{\partial x}\right)_{i+1/2} - \left(\kappa_{eq}\frac{\partial T}{\partial x}\right)_{i-1/2}\right]\Delta y\,, \quad 1 \tag{8}$$

$$\textit{Net y-diffusion} = \left[\left(\kappa_{eq}\frac{\partial T}{\partial y}\right)_{j+1/2} - \left(\kappa_{eq}\frac{\partial T}{\partial y}\right)_{j-1/2}\right]\Delta x\,.$$

The results for the energy budget are presented in Figs. (7) and (8). These results correspond to a cavity of aspect ratio equal to eight. The entrance velocity is set to 8 m/s, corresponding to Res = 21,255. The temperature at the entrance section is uniform, T_{in} = 300 K. The same value was enforced at solid walls, except at the cavity floor, where T_w = 350 K. The control volumes adopted have a length Δx and cover all the cavity height, i.e., from y = 0 until y = s (see fig. (6)). In this way we take into account the mean effect of convection and diffusion along the cavity height and its local variation along cavity length.

Noticeable, the most interesting aspect that may be observed in fig. (7) is the symmetrical behavior for the convection fluxes along x and y directions. Besides, the convection terms have greater magnitude than the diffusion terms (see fig. (8)). In spite of this fact, the net contribution due to convection (summing up x and y fluxes) has the same order of magnitude than y-diffusion term. This is so because for a steady state problem without heat sources, the energy conservation principle states that net energy entering or leaving the control volume by convection must be equal its counterpart by diffusion. It interesting to note that in this case (cavity with aspect ratio 8) we have two bubbles encapsulated inside the cavity, i.e., the flow does not reattach at the cavity floor (Zdanski et al., 2003; 2005). Perhaps, this is the reason for the symmetrical behavior of convection fluxes in the energy budget. Furthermore, from Fig. (8), we realize that the y-diffusion term is more important than its counterpart in the x-direction.

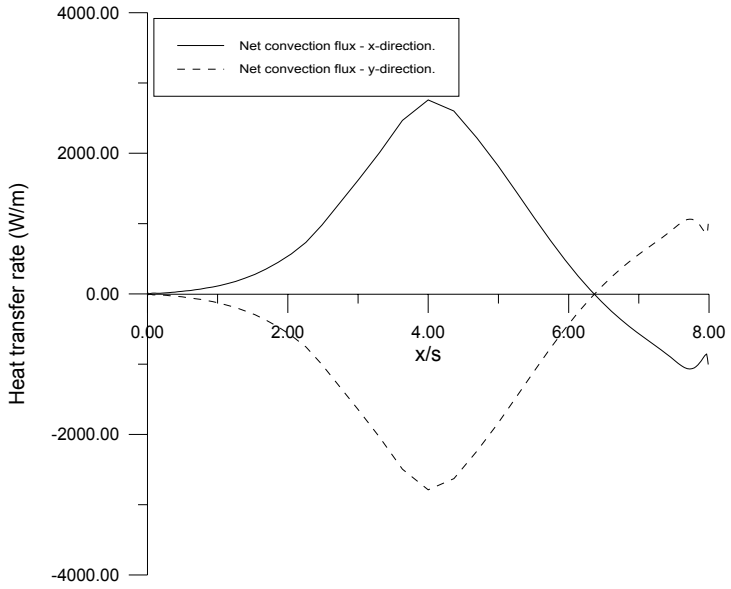

Figure 7. Net convection fluxes inside the turbulent cavity with aspect ratio 8.

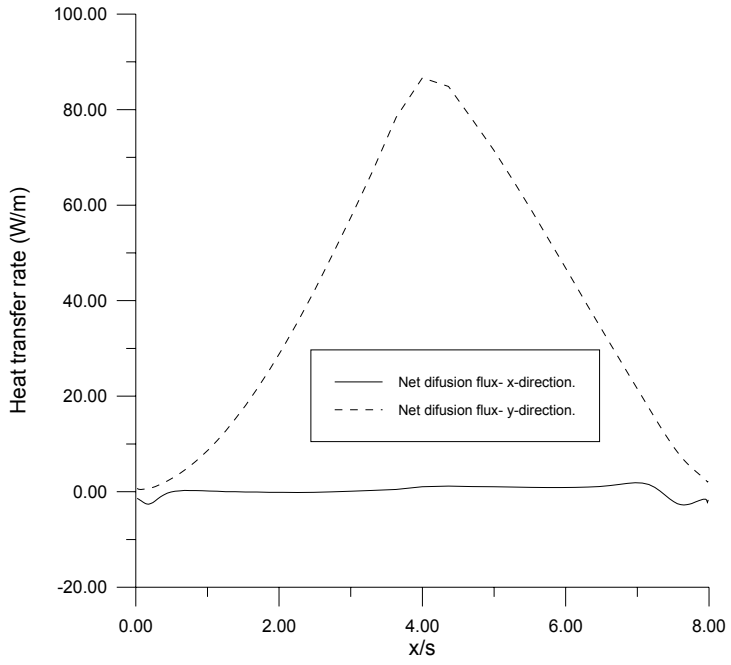

Figure 8. Net diffusion fluxes inside the turbulent cavity with aspect ratio 8.

4. Conclusions

The results presented help to clarify some interesting aspects of the incompressible flow over shallow cavities. The vorticity shed at the upstream corner and the stagnation region formed at the downstream vertical face has a major influence on vortices position inside the cavity. For the turbulent regime, the effect of vorticity is less important than in the laminar case. This basically explains the opposite behavior of the bubbles inside the cavity as function of the Reynolds number. Furthermore, the energy budget inside the cavity shows an interesting aspect related with the net convection fluxes inside the cavity, i.e., the symmetrical behavior.

5. References

Frigo, L. M., Mansur, S. S., Campregher, R., De Arruda, J. M. and Silveira Neto, A., 2004, "Análise Numérica de Escoamentos Sobre Cavidades Abertas Bidimensionais", Proceedings of the 10th Brazilian Congress of Thermal Science and Engineering, Rio de Janeiro, Brazil.

Launder, B. E. and Spalding, D. B., 1974, "The Numerical Computation of Turbulent Flows", Computer Methods in Applied Mechanics and Engineering, Vol.3, pp. 269-289.

Mansour, N. M. and Kim, J. and Moin, P., 1983, "Computation of turbulent flows over a backward-facing step", Nasa Technical Memorandum, 85851.

Patankar, S. V., 1980, "Numerical Heat Transfer and Fluid Flow", McGraw-Hill Book Company, New York, EUA, 196 p.

Sinha, S. N., Gupta, A. K. and Oberai, M. M., 1982, "Laminar Separating Flow over Backsteps and Cavities part II: Cavities", AIAA Journal, Vol.20(3), pp. 370-375.

Zdanski, P. S. B., Ortega, M. A. and Fico JR, N.G.C.R., 2003, "Numerical Study of the Flow over Shallow Cavities", Computers & Fluids, Vol.32(7), pp. 953-974.

Zdanski, P. S. B., Ortega, M. A. and Fico JR, N.G.C.R., 2004, "Numerical Simulation of the Incompressible Navier-Stokes Equations", Numerical Heat Transfer Part B: Fundamentals, Vol.46(6), pp. 459-479.

Zdanski, P. S. B., Ortega, M. A. and Fico JR, N.G.C.R., 2005, "Heat Transfer Studies in the Flow over Shallow Cavities", Journal of Heat Transfer (ASME), Vol.127(7), pp. 699-712.

6. Copyright Notice